ChemPubSoc Europe

DOI: 10.1002/celc.201901976

CHEMELECTROCHEM Articles

Special Collection

Array Microcell Method (AMCM) for Serial Electroanalysis

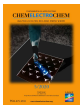

Sasha E. Alden, Natasha P. Siepser, Jacqueline A. Patterson, Gargi S. Jagdale, Myunghoon Choi, and Lane A. Baker*[a]

Dedicated to Prof. Richard M. Crooks on the occasion of his 65th birthday

We describe a method for electrochemical measurement and synthesis based on the combination of a mobile micropipette and a microelectrode array, which we term the array microcell method (AMCM). AMCM has the ability to address single electrodes within a microelectrode array (MEA) and provides a simple, low-cost format to enable versatile electrochemical measurements. In AMCM, a droplet at the tip of a movable micropipette (inner diameter of 50 μm) functions as an electrochemical cell, in which the electrode area is defined by a microelectrode of the array. We also report carbon MEAs that are well suited for AMCM and are fabricated from pyrolyzed photoresist films (PPFs). PPF-MEAs with nominal electrode diameters of 5.5 μm are characterized by AMCM, standard macroscale electrochemical methods, and finite element modeling. The versatility of AMCM is demonstrated by measurement of single Pt microparticles and by electrodeposition of shape-controlled Pt nanoparticles.

1. Introduction

Over the last decade, the race to true nanoscale electrochemical imaging has resulted in development of a number of ground breaking techniques for measuring electrochemistry at small scales. These include, scanning electrochemical microscopy (SECM),[1] scanning ion conductance microscopy (SICM),[2] scanning electrochemical cell microscopy (SECCM),[3] scanning electrochemical microscopy-atomic force microscopy (SECM-AFM),[4] and variations/combinations thereof.[5] With these techniques, the importance of small scale, correlative approaches between electrochemical measurements and secondary techniques have also grown. This combination, small scale electrochemistry and supporting measurements, so-called "correlative multi-microscopy" approaches, has proven especially powerful for elucidating new information in nano- and microelectrochemical systems.[6] Arrays provide a powerful tool to enable the bridge between different microscopy modes, and have found wide application, for instance in the combination of SECCM with transmission electron microscopy (TEM) and scanning electron microscopy (SEM).[6-7] In these experiments, the array is typically an electron microscopy grid, which serves to collocate sample features.[3a,8] An alternative to high resolution imaging approaches, one that offers significant advances in terms of instrumental simplicity, is to instead create an array of small electrodes, which can then be addressed individually by a moving microcell (micropipette) approach. Here, we develop such a tool, which we term the Array MicroCell Method (AMCM). AMCM, as employed here, makes use of a pyrolyzed photoresist film (PPF) carbon electrode fabricated in a microelectrode array (MEA) format to generate pyrolyzed photoresist film-microelectrode arrays (PPF-MEAs), with a number of beneficial properties for both electroanalytical measurements and materials synthesis. In this report, we describe operation of AMCM with PPF-MEAs and highlight the advantages provided, in particular for single particle measurements and the electrodeposition of shaped nano/microparticles.

AMCM is the progeny of a number of micropipette contact based methods developed starting around 1995 by Bohni.[9] Initial efforts at droplet based electrochemical measurements involved a stationary pipette, termed "microcell," and correlative optical microscopy with the cell area defined by a silicone rubber gasket. Soon after, scanning[10] and feedback modes[11] were introduced by Lohrengel and Bonhi, respectively. In 2009, Williams and co-workers developed scanning micropipette contact method (SMCM) which used 1.5 um pipettes and included full feedback and scanning capabilities.[12] Variations on SMCM have produced a body of scanning droplet work including battery investigations,[13] nanopore modification/characterization,[14] and electrodeposition.[7,15] Recently, investigation of oxygen evolution catalysis was performed using a scanning droplet technique on an array of inkjet-printed catalysts.[16] Micropipette contact methods have led to what might be the ultimate resolution for such a technique, with nanoscale droplets employed by SECCM.[3a,17]

In the technique presented here, AMCM, we use PPF-MEAs to our advantage in correlative microscopy characterization. Here, we employ carbon electrodes – an electrode material which is often chosen for catalytic and/or bioanalytical studies – prepared in microscale arrays.[18] PPF carbon electrodes are constructed by pyrolysis of photoresist at high temperatures and combine the typical advantages of carbon electrodes – wide potential windows, chemical inertness and biocompatibility with low surface roughness. PPFs can also be mass produced in numerous dimensional patterns,[18a] with the added benefit of

[a] S. E. Alden, N. P. Siepser, J. A. Patterson, G. S. Jagdale, M. Choi, Dr. L. A. Baker
Department of Chemistry, Indiana University
800 E Kirkwood, Bloomington, 47405, Indiana (USA)
E-mail: lanbaker@iu.edu

Supporting information for this article is available on the WWW under https://doi.org/10.1002/celc.201901976

Special Collection *An invited contribution to the Richard M. Crooks Festschrift*

renewal by fast scan cyclic voltammetry (FSCV)[19] or heat treatments.[20]

MEAs can be fabricated in a wide range of dimensions, electrode size and spacing,[21] which provide low single-to-noise, small iR drop and spatial registry.[22] Individually addressable arrays are highly desirable, but pose fabrication challenges and require more involved electronics, especially when dense, small electrodes are arrayed.[23] Commercial MEAs have started to emerge, but are often expensive and limited in configurational flexibility. AMCM has the capability to assess single electrodes within an array without complex electronics or electrode connections. Here, we take advantage of PPF-MEAs, our array of choice, for AMCM to measure single particles and electrodeposit shaped nano/microparticles.

2. Results and Discussion

Fabrication of PPF-MEAs was carried out with standard photolithography techniques (Figure 1a) to produce films with properties in good agreement with previous reports.[18a] First, a positive photoresist was applied to a Si/SiO_2 wafer and then pyrolyzed under an atmosphere of forming gas to obtain a PPF with nominal thickness of 1.5 ± 0.3 μm, sheet resistance of 51.2 Ω/□, and low RMS roughness (0.80 nm over a 10×20 μm area). A second layer of photoresist was then spin-coated on top of the PPF and developed to define the PPF-MEAs (Figure 1a). PPF-MEAs fabricated for this work had an electrode diameter of ca. 5.6 μm with electrode spacing (d) of 150 μm. Cyclic voltammetry (CV) of differently spaced PPF-MEAs are included in the SI where the diffusion profile changes from planar to radial at increasing d/a (a = electrode radius) values (Figure S1a).[24] Standard macroscale electrochemical characterization of PPF-MEAs revealed a typical steady-state response at slow scan rates with increasing Cottrellian behavior at faster scan rates (Figure S1b).[24] The AMCM setup consisted of a two-electrode circuit connected to a potentiostat (Figure 1b). PPF-MEAs acted as the working electrode and a quasi-reference counter electrode (QRCE), typically a Ag/AgCl or PdH_2 wire, back inserted into a solution-filled borosilicate pipette (I.D. 50 μm, Figure 1c inset) completed the circuit. This solution filled pipette was then positioned at a single electrode within a MEA, via micromanipulators and optical cameras to visualize the MEA and pipette easily (Figure 1c). Once the droplet at the tip of the pipette made contact with the surface, a measurement was collected, and the position manually recorded. In the AMCM configuration, the microelectrode defines the electrode area, while the droplet defines the electrochemical cell.

To quantify the electrochemical behavior of a PPF, voltammetric studies were carried out at the macro- and nanoscale with the inner-sphere redox probe $FcTMA^+$. The macroscopic voltammetric response (Figure 2a) is shown on a PPF and glassy carbon (GC) electrode, where the similarity in response suggests good electrochemical performance for PPFs, further confirmed in the linear relationship of the anodic peak current (i_{pa}) vs. scan rate ($v^{1/2}$) (Figure 2a, inset). Nanoscale voltammetric responses at these carbon electrodes were also characterized by SECCM, a technique previously employed to study highly oriented pyrolytic graphite[25] and screen printed carbon electrodes.[26] Herein, the droplet at the tip of a solution filled nanopipette, O.D. 150–250 nm, was brought in contact with the electrode surface at a series of predefined positions and a CV was recorded at each point to construct a map. A SECCM map, showing the current response at 0.6 V vs Ag/AgCl, on PPF (Figure 2b) and GC (Figure S2) electrodes demonstrated minimal variations in current response between pixels, ca. < 4 pA,

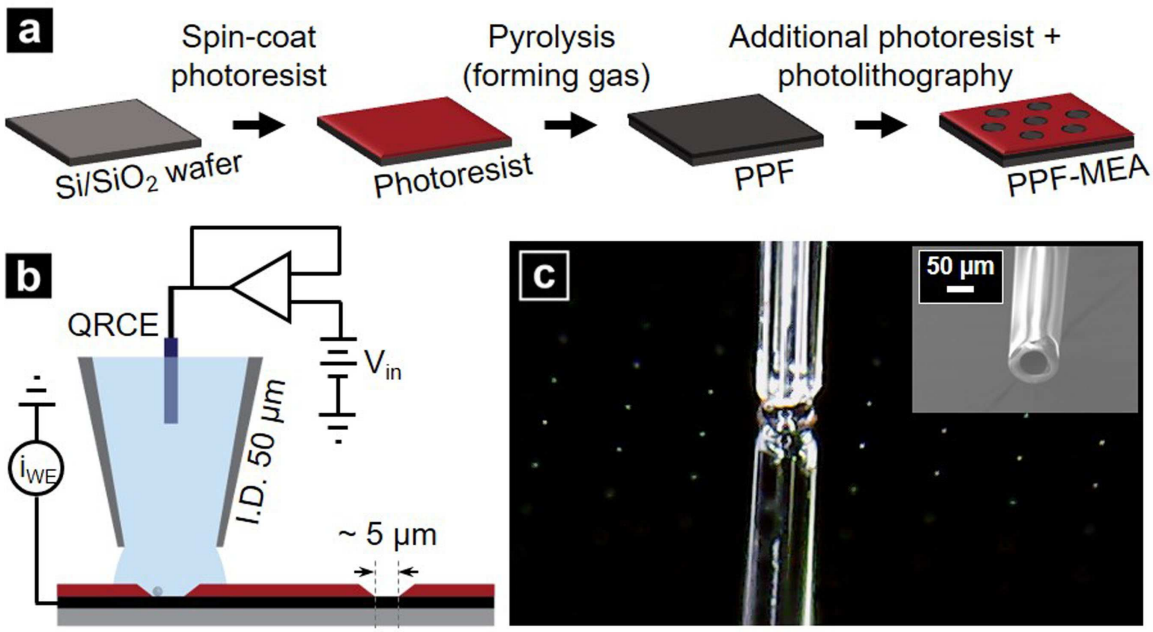

Figure 1. a) Scheme of pyrolyzed photoresist film-microelectrode array (PPF-MEA) fabrication. b) AMCM electrochemical measurement setup. c) Optical image of AMCM, where bright spots are microelectrodes 150 μm apart. The inset shows an electron micrograph of a typical pipette used.

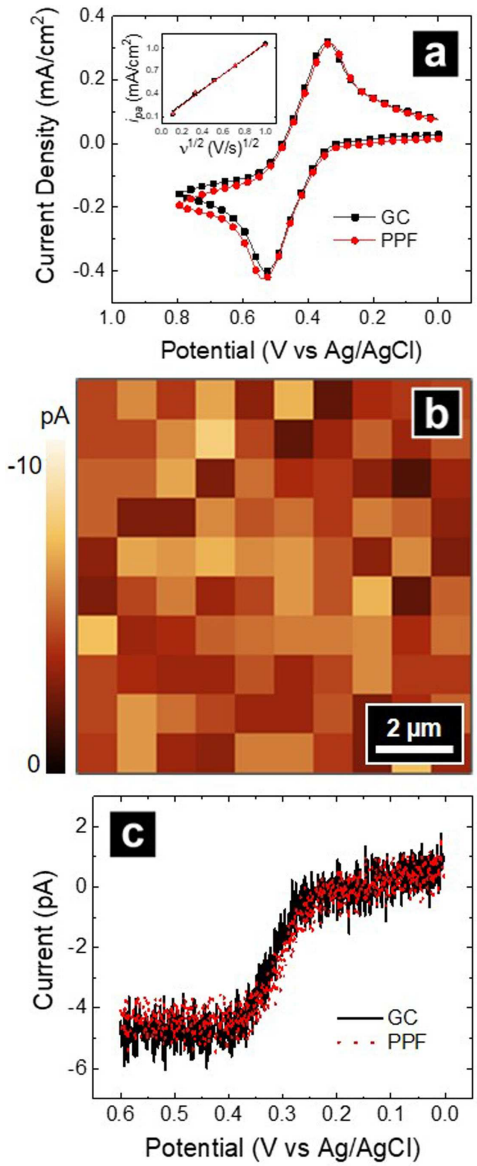

Figure 2. a) Cyclic voltammograms of 2 mM $FcTMA^+$ at 0.1 V/s with 0.1 M KCl as the supporting electrolyte on PPF and GC electrodes. Inset plot of peak anodic current vs $v^{1/2}$ is included to illustrate similarity in response of the two electrodes. b) SECCM CV map at 0.6 V vs Ag/AgCl on a PPF. c) Average SECCM CV response at a glassy carbon (black) and PPF (red) substrate. For SECCM, the solution in the pipette was 2 mM $FcTMA^+$ in 50 mM KCl, the scan rate was 1.2 V/s, and the pixel resolution was 1 µm/pixel.

suggesting a comparable and homogeneous electrochemical response at electrode surfaces. The average SECCM CV response, collected at three different locations (more information in Figure S2), at PPF and GC showed a steady-state, mass-transport limited current response (Figure 2c), indicative of quasi-radial diffusion to a planar surface,[27] with limiting currents of ca. 5 pA for both substrates. These data sets suggest the PPFs, as prepared here, provides a suitable material for further MEA development.

Validity of AMCM was demonstrated by comparison of cyclic voltammograms of FcMeOH between the same isolated, individual microelectrode, (i.e. not within an array) measured by AMCM, by solution immersion of the electrode, and characterized by finite-element simulations of a single microelectrode of the same dimensions (Figure 3). The single microelectrode examined (Figure 3a) was 5.6 µm in diameter with conical side walls at an angle of ca. 45° from the surface (defined as the angle between the surface normal and sidewall) and a recess depth (L) of 2.25 µm as measured by atomic force microscopy (AFM) (Figure 3a–b). A CV was collected using an immersed custom Teflon cell (exposed area of 0.31 cm^2), with the electrochemically active area defined by the single electrode at the center. Next, on the same electrode, an AMCM measurement was carried out and the current response for both AMCM and the immersed, macroscale measurement are shown in Figure 3c. Comparison of the response at these experimental scales is important to confirm and underscore the direct parallel between standard electrochemical methods and AMCM. Similar steady-state current is observed for both measurement approaches. This result is indicative that the AMCM response faithfully reports the electrochemical response that would be recorded in a typical experiment. Additional AMCM measurements with FcMeOH are shown in Figure S3, and show consistency between CVs when the pipette is repeatedly approached and retracted from the surface between each measurement.

Microelectrodes in the PPF-MEAs can be described as a conical well, or as a conically recessed ultramicrodisk electrode (CRUME).[28] This sidewall/electrode geometry was found to be beneficial for droplet-electrode contact for surfaces and liquids employed here. The steady-state current response for such an electrode, lies between the classic inlaid microdisk and a recessed microdisk.[22e,29] Thus, current values are always fractional of the microdisk relationship commonly described,[30] in which the steady-state current, i_{ss}, is dependent on the number of electrons transferred, n, Faraday's constant, F, electrode radius, a, the diffusion coefficient, D, and concentration, C, of the redox species [Eq. (1)].

$$i_{ss,\ \mathrm{microdisk}} = 4nFaDC \quad (1)$$

A conical well electrode depends on these parameters, plus two additional parameters, the depth of the well (similar to the depth of a recessed microdisk) and the conical angle. To our knowledge, the interdependent variation in multiple geometric factors makes it difficult to derive a general analytical expression, and as such finite element simulations are typically employed for geometries similar to the conical well. Britz and Strutwolf carried out detailed simulations to treat the conical well geometry which provide an excellent generalized picture of mass transport effects in this restricted geometry, where the transitions from radial to linear diffusion are highly dependent on well depth and cone angle.[28] Finite element simulations (COMSOL) were performed for the exact electrode geometry characterized in Figure 3a–c. Simulations of the cyclic voltammetric response of a conical well microelectrode with 2 mM FcMeOH in 25 mM KCl solution as a function of cone angle are shown in Figure 3d (see SI for modeling details). Simulation at a

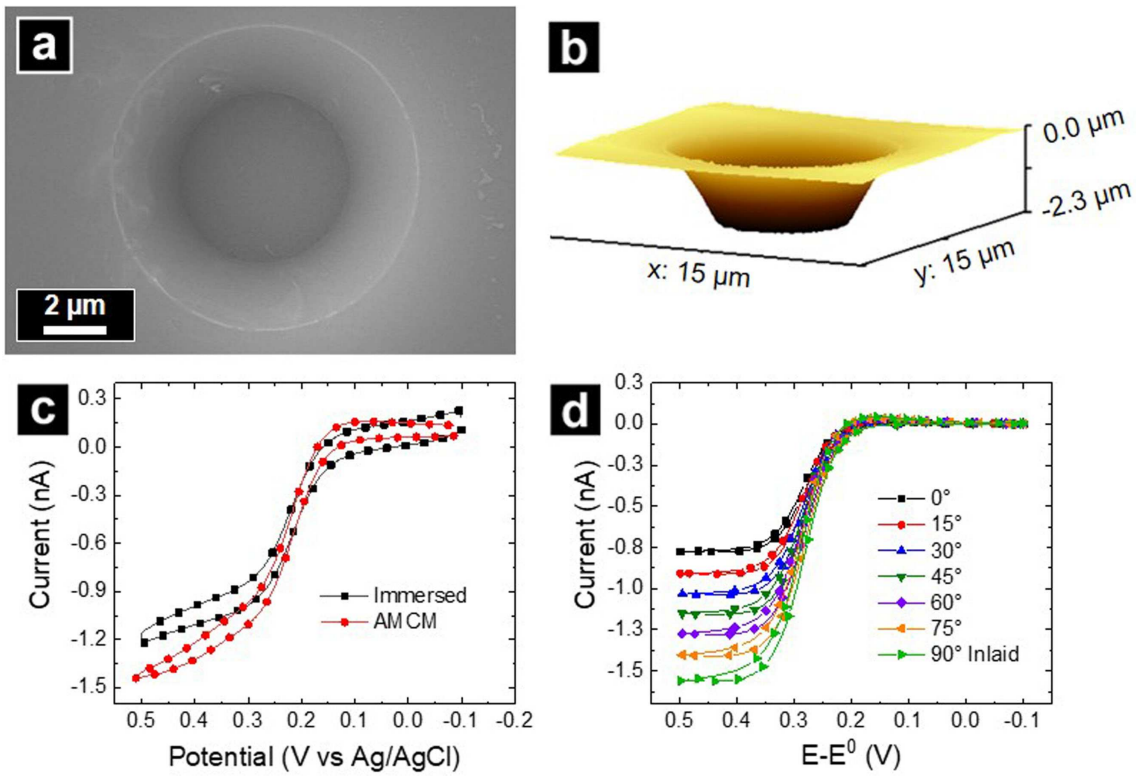

Figure 3. Electron micrograph (a) and AFM (b) of an individual microelectrode. c) Cyclic voltammograms for FcMeOH oxidation when immersed and by AMCM of the same single 5.6 µm diameter microelectrode at 0.05 V/s. The solution was 2 mM FcMeOH and 25 mM KCl. d) Finite-element simulations of AMCM measurements with varying conical side wall angles.

cone angle of 45° agrees with the result for the immersed electrode measured in Figure 3c. The AMCM measurement is close but is ca. 17% higher than both the simulation and the immersed electrode. There are a number of parameters estimated in the drop dimension which are difficult to determine precisely and could lead to this subtle difference. These parameters are, principally, droplet dimension/shape, separation between the micropipette tip and electrode surface, and contact angles of the electrolyte solution at the electrode and micropipette surfaces. Additional simulations of these geometric features (Figure S4) did not immediately identify the origin of the discrepancy, and a more detailed simulation study is presently underway.

To demonstrate the utility of AMCM, single particle measurements were carried at electrodeposited Pt particles. A PPF-MEA was immersed in a solution of 2 mM K_2PtCl_6 and 0.1 M H_2SO_4, and a potential program (Figure 4a) was applied to deposit Pt particles. First, the potential was stepped from an inert potential (E_1) to a reducing potential (E_2) to generate Pt nuclei in the electrodes within the PPF-MEA at a time duration t_1 and t_2, respectively. Then, a square wave program was implemented where the potential oscillated between an oxidizing (E_{Ox}) and a reducing potential (E_{Red}) at a frequency (f) of 100 Hz for a set time (t_3) to grow and shape the Pt particles. The particle shape can be altered by changing E_{Ox} and E_{Red}.[31] The bulk electrodeposition, was performed with the following parameters with respect to a Ag/AgCl (3 M NaCl) reference: E_1 = 0.41 V, t_1 = 1 s, E_2 = 0.34 V, t_2 = 0.4 s, E_{Ox} = 0.61 V, E_{Red} = 0.21 V, f = 100 Hz, and t_3 = 45 min.

This deposition program created spherical, ca. 2 um diameter, Pt microparticles in approximately 78% (1-3 particles) and 43% (single particle) of exposed electrodes (n = 60, Figure 4b). An electrode containing one Pt microparticle (Figure 4c) was then characterized for hydrogen adsorption/desorption by underpotential deposition (H_{UPD}) in 0.01 M $HClO_4$ by AMCM vs PdH_2 QRCE (Figure 4d). Particles were first cycled 3 times at 200 mV/s from 0 to 1.2 V starting at 0.4 V to remove any contamination and remove surface Pt oxide species. Then, 2 additional H_{UPD} cycles were recorded, the 2nd cycle is shown in Figure 4d. A similar procedure was used by Crooks and co-workers to ensure an accurate and consistent measurement.[32] One set of H_{UPD} peaks is observed for particles examined here, a response consistent with a previous single particle study.[32] Location of H_{UPD} and Pt oxide reduction/oxidation peaks correlate with Pt surfaces from previous reports.[32–33] Electrochemical surface area was calculated by integration of Pt oxide peak present at ca. 0.6 V vs PdH_2 (* in Figure 4d) with conversion value of 420 µC/cm.[34] Calculated active surface area was 14 times greater than that of a platinum sphere of the same dimension. This assumes a smooth/solid Pt particle, which may well not be the case for the example shown here, however, such high surface area particles are of interest for future studies of catalysis. These measurements demonstrate the utility of the AMCM for studies at single entities, such as individual electro-

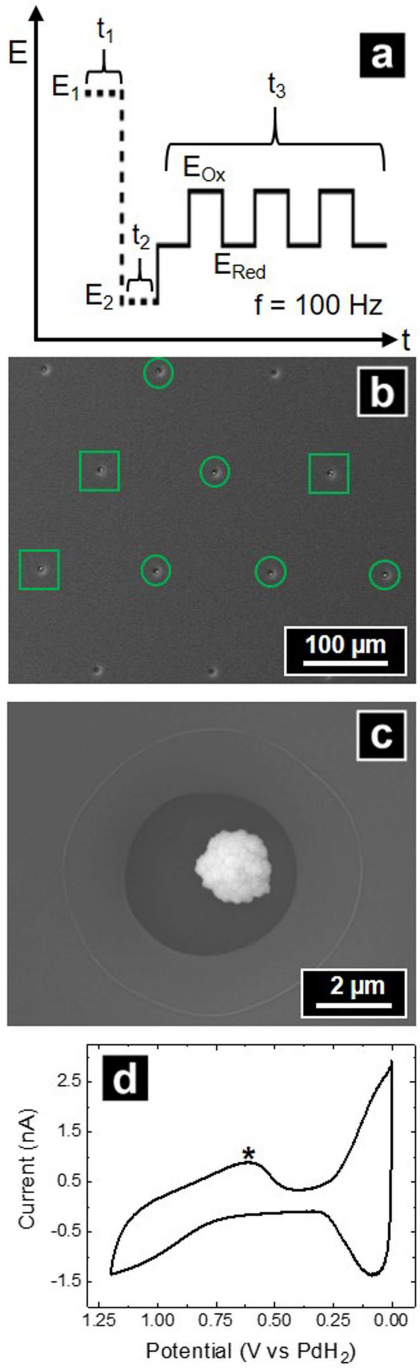

Figure 4. a) Schematic of Pt electrodeposition potential step program. Electron microscopy images of b) the Pt particle distribution on a PPF-MEA and c) an electrode with a single Pt particle. The green circles and squares in (b) highlight electrodes containing one and two Pt particles, respectively. d) A cyclic voltammogram at the electrode from (c) in 0.01 M $HClO_4$ at a scan rate of 200 mV/s.

des or particles. AMCM clearly permits addressing individual electrodes, obviating the need for complicated microfabrication of electrode leads.

In addition to single-entity measurements, AMCM is a useful tool for high-throughput screening of conditions for electrodeposition of nanoparticles, where the droplet functions as a reaction vessel to deposit and grow particles. With consideration that metal electrodepositions can prove sensitive reactions, which can be difficult to optimize, the ability to screen deposition parameters and repeat conditions many fold over is very attractive. Since Tian et al. introduced a protocol for the electrochemical deposition and shaping of Pt to yield particles with high-index facets,[35] there have been many publications reporting the deposition of Pt particles with different morphologies.[31,33a,36] Here, we adopted the electrochemical Pt particle deposition method (similar to that described above) for Pt nanoparticle (Pt NP) deposition by AMCM, proceeded by morphology characterization with SEM (Figure 5). The following parameters, with respect to PdH_2 QRCE, were used to deposit Pt NPs as shown in Figure 5a: $E_1 = 0.19$ V, $t_1 = 1$ s, $E_2 = -0.12$ V, $t_2 = 1$ ms, $E_{Ox} = 0.96$ V, $E_{Red} = -0.18$ V, $f = 100$ Hz, and $t_3 = 10$ s. Shaping potentials, E_{Ox} and E_{Red}, were then increased by 20 mV going from left to right and top to bottom respectively (as indicated by arrows Figure 5). Under these conditions, each electrode of the array was filled with particles to the edge, or near edge, of the electrode boundary, which strongly suggests good wetting by the droplet, in agreement with the electrode characterization described *vide supra*. A rarely occurring "bald spot" can be seen on the left-hand side of the electrode in Figure 5a. This is likely due to a small amount of remaining photoresist on the surface of the PPF within the electrode area.

By varying E_{Ox} and E_{Red} systematically in a grid pattern, a trend in particle faceting was generated. As E_{Ox} was increased, the Pt NPs became more cubic as evidenced by the transition towards sharper edged particles from columns a to c in Figure 5. Particles in selected electrodes on the array were characterized by measuring the aspect ratio, where a value of 1 indicates a perfect square and 0 a line, and circularity, where a value of 1 indicates a perfect circle and 0.78 a perfect square, with image analysis software (see SI shape descriptors). Due to the high density of particles, only isolated particles were considered. Comparison of individual particles within the inset images in Figure 5a and 5c, revealed an aspect ratio of 1.17 ± 0.18 and 1.08 ± 0.04 and circularity of 0.56 ± 0.09 and 0.63 ± 0.07, respectively (Figure 5, S5, SI shape descriptors). In combination, the aspect ratio and circularity confirm that the particles shown in Figure 5c are more cubic than in 5a. When E_{Red} is increased, higher index faceting began to appear, where the occurrence of clear pyramidal additions to the sides of the larger cubic structures are observed. The trend towards more complex faceting as E_{Ox} and/or E_{Red} were increased was consistent with work from the Sun Group.[31] Also of note, Pt electrodepositions via AMCM are different than bulk electrodepositions because of faster mass transport with AMCM, as seen with ultramicroelectrodes[32] and SECCM.[8b] Consequently, AMCM has the advantages of reduced electrode fabrication/preparation time and faster depositions, which drastically increases throughput of parameter vetting.

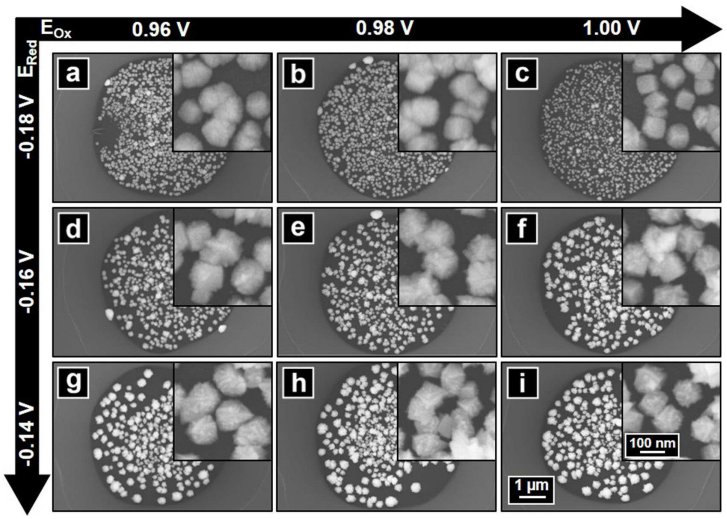

Figure 5. Microscopy images of electrodeposited Pt nanoparticles by AMCM in microelectrodes on a PPF-MEA. Values for E_{ox} and E_{Red} correspond to the waveform shown in Figure 4a.

3. Conclusions

In this report, we detailed operation of AMCM with PPF-MEAs. AMCM provides several attractive advantages worth note. First, AMCM allows addressing individual elements in a MEA in a simple and straightforward fashion without the need for complex electrode connections. Further, if the drop size is large relative to the size of the electrode and the spacing between the electrodes is sufficient, simple optical interrogation is sufficient to position the micropipette and contact an individual electrode. With this approach, and a single experiment setup, many individual experiments or replicant measurements can be performed in a short amount of time. We also describe carbon electrode arrays which are suitable for AMCM, and provide low roughness, inert electrodes for synthesis of electrocatalytically interesting materials. PPF-MEAs were suitable for both single entity preparations and interrogation, and for electrodeposition of shaped nanoparticles. Shape-controlled nanoparticle studies demonstrated that AMCM with PPF-MEAs is highly commensurate with correlative microscopy approaches and integrates easily into correlative electrochemical/electron microscopy approaches. In the future, we posit that these same electrodes will also prove suitable for single entity measurements in biological studies, such as single cells.

Finally, for work reported here, positioning of the AMCM probe was achieved either with a manual micromanipulator or a motorized, but still manually controlled, micromanipulator. Feedback control in movement of the probe to the surface can be easily incorporated and if array elements are evenly spaced, the entire process can be automated with very simple (relative to state-of-the-art) positioning hardware, to enable high throughput electrochemical studies that can take advantage of correlative microscopy approaches. This work is presently underway in our laboratories and will be reported in due course.

Experimental Section

Chemicals and Materials

Deionized water (Resistivity = 18.2 MΩ cm at 25 °C, Millipore Sigma, Burlington, MA) was used to prepare all solutions. Potassium hexachloroplatinate (IV) (K_2PtCl_6, 98%, Sigma Aldrich, St. Louis, MO), sulfuric acid (H_2SO_4, Marcon Chemicals, Randor, PA), potassium chloride (KCl, VWR Analytical, Randor, PA), potassium nitrate (KNO_3, EMD, Burlington, MA), hyrdroxymethylferrocene (FcMeOH, 99%, Strem Chemicals, Newburyport, MA) and perchloric acid ($HClO_4$, Fisher Scientific, Hampton, NH) were used as received. A metathesis reaction was used to convert (ferrocenylmethyl) trimethylammonium iodide ($FcTMA^+I^-$, Strem Chemicals) to (ferrocenylmethyl) trimethylammonium hexafluorophosphate ($FCTMA^+PF_6^-$). The resulting hexafluorophosphate salt was dried and stored at room temperature prior to use. Glassy carbon (Alfa Aesar, Haverhill, MA) electrodes were polished with 0.05 µm alumina powder (CH Instruments, Austin, TX) and sonicated in water prior to use.

Electrode Preparation

PPFs-Positive photoresist (Microposit S1813, DOW, Marlborough, MA) was used to create conductive carbon films (PPF). Silicon oxide coated Si wafers (Si/SiO_2) (University Wafer, South Boston, MA) were used as substrates. Si/SiO_2 wafers were first sonicated for 10 mins in ultrapure water and isopropanol, respectively, and dried under a stream of dry nitrogen. Immediately before applying photoresist; substrates were heated on a hotplate at 120 °C for 5 min to allow surface water to evaporate. Two coats of photoresist was applied with a spin coater (Headway Research Inc. Model PWM50, Garland, TX) to a room temperature Si/SiO_2 wafer. Pyrolysis was performed in an air-free tube furnace (Lindberg, Riverside, MI) at 900 °C for 60 min with a 20 °C/min ramp under a constant flow of forming gas (95% N_2, 5% H_2). Final PPFs had a thickness of 1.5 ± 0.2 µm, sheet resistance 51.2 Ω/□, and a RMS roughness of 0.8 nm.

Microelectrode arrays- An additional single coating of S1813 was applied to PPFs to a thickness of 2.6 ± 0.1 µm (L). Photolithography was performed with a mask aligner (OAI, San Jose, CA) as specified

by the manufacturer to create PPF-MEAs with an electrode radius (a) of 2.8 μm and electrode spacing (d) of 150 μm.

Macroscale Characterization of PPF-MEAs

SEM images were collected on a Carl Zeiss Auriga FIB-SEM (Oberkochen, Germany). PPF sheet resistance (51.2 Ω/□) was determined by a 4-point probe (MMR Technology Inc, San Jose, CA). Measurements were made with 4 in-line probes with an average spacing of 2.5 mm. Film thickness was measured using a KLA Tencor P7 surface profiler (1.5 ± 0.3 μm PPF, 2.6 ± 0.1 μm MEA) and PPF RMS surface roughness (0.8 nm) was determined by non-contact mode AFM (XE-Bio, Park System, South Korea) over a 10× 20 μm area with PPP-NCHR cantilever with 20 nm tip diameter.

Macroscale electrochemical characterization of PPFs and PPF-MEAs was performed using cyclic voltammetry (CV) by CHI 910b potentiostat (CH Instruments, Austin, TX) with 0.312 cm^2 exposed electrode area in a custom Teflon cell. A counter electrode made from Pt mesh (99.9% purity, 152 wires/inch) and Pt wire (99.99% purity, 0.6 mm diameter) were purchased from Goodfellow (Coraopolis, PA). A Ag/AgCl (3 M NaCl) reference electrode was purchased from BASi (West Lafayette, IN).

AMCM

AMCM setup (Figure 1) used either, a Ag/AgCl wire or PdH_2 wire (0.003″ diameter, California fine wire, Beach Grove, CA) as the quasi-reference counter electrode (QRCE). A CHI 910b potentiostat (CH Instruments, Austin, TX) was used to apply the potential between the QRCE and a PPF-MEA, which served as the working electrode in two-electrode system. Borosilicate pipettes were fabricated from 1.0 mm outer diameter (O.D), 0.58 mm inner diameter (I.D.) capillaries with a flaming brown P-97 filament puller (Sutter Instruments, Novato, CA). Capillaries were first pulled to pipettes with a long shank using the following parameters: heat = 715, pull = 0, velocity = 150 and time = 0. Then the "glass-on-glass" method was used as specified in the Sutter Pipette Cookbook (2018) to fabricate pipettes with I.D. of 52 ± 2.7 μm. Pipette was positioned using a Zaber T-JOY3 series joystick (Zaber, Vancouver, BC, Canada), which controlled a 3 axis x, y, z positioning system. Pipette position was determined by two optical cameras and electrode location was recorded manually.

SECCM

Quartz pipettes were fabricated from dual barrel capillaries with 1.2 mm OD and 0.90 mm ID with a P-2000 laser puller (Sutter Instruments, Novato, CA). Pulled pipettes resulted in an approximate OD of 200 nm and an ID of 75 nm per barrel. Pipettes were filled with 2 mM $FcTMA^+$ with 50 mM KCl. Perfluoroalkoxy (PFA, A–M Systems, Sequim, WA) coated silver wires were used to make Ag/AgCl QRCEs by stripping off the coating to expose the silver wire and subsequently chloridizing the Ag wire. Chloridized silver wires, which serve as QRCEs, were inserted into each barrel of the pipette. Our SECCM instrumentation setup is described in detail elsewhere.[3a] In brief, a commercial Park Systems Dual AFM/SICM (Suwon, Korea) instrument was modified by the addition of a current amplifier (CHEM-CLAMP, Dagan Corp., U.S.A.) equipped with a 100 MΩ headstage and custom potentiostat, designed in-house. During SECCM, a 100 mV bias was applied between the QRCEs to generate an ion conductance current for SECCM feedback. The pipette was oscillated at a frequency of 1000 Hz with an oscillation height of 20 nm. AC hopping mode was used for SECCM CV mapping were the lift height, pixel resolution, and scan rate were 500 nm, 1 μm/pixel, and 1.2 V/s, respectively.

Pt Electrodeposition and Shaping

Electrochemical measurements were performed using a CHI 660 and CHI 910b potentiostat (CH Instruments, Austin, TX). All depositions were carried out in 2 mM K_2PtCl_6 and 0.1 M H_2SO_4. Immersed, macroscale Pt depositions resulting in 1–3 Pt particles deposited into each electrode on the PPF-MEA were prepared by the following potential step program vs Ag/AgCl (3 M NaCl): E_1 = 0.41 V, t_1 = 1 s, E_2 = 0.34 V, t_2 = 0.4 s, E_{Ox} = 0.61 V, E_{Red} = 0.21 V, f = 100 Hz, and t_3 = 45 min. This program yielded Pt particles with diameters of ca. 1–2 μm.

Pt deposition and growth of faceted particles using AMCM were carried out with a 2 mM K_2PtCl_6 and 0.1 M H_2SO_4 filled pipette. The following parameters vs PdH_2 were used to deposit particles show in Figure 5a: E_1 = 0.19 V, t_1 = 1 s, E_2 = −0.12 V, t_2 = 1 ms, E_{ox} = 0.96 V, E_{red} = −0.18 V, f = 100 Hz, and t_3 = 10 s. $E_{ox\ and}$ E_{red} were increased by 20 mV going from left to right and downward respectively (Figure 5). Electrode position was then recoded and particles were characterized by SEM (Figure 5).

Acknowledgements

Prof. Cathrine Reck is acknowledged (Indiana University) for access to tube furnaces used in carbon electrode preparation. Ms. Kristen Alanis is acknowledged for her help with pipette characterization by SEM. The IU Nanoscale Characterization Facility is acknowledged for access to and use of the cleanroom facilities and scanning electron microscope, FIB (acquired through the National Science Foundation MRI program (0923064)). Instrumentation developed here is in support of single entity studies through NIH grant 1R01NS105888-01. Prof. Shixiong Zhang, Dr. Wencao Yang, and Amanda Coughlin from IU Department of Physics are acknowledged for their help with the four-point probe measurements. Access to computational facilities at Indiana University is supported in part by Lilly Endowment, Inc., through its support for the Indiana University Pervasive Technology Institute.

Keywords: microarrays · scanning probe microscopy · cyclic voltammetry · nanoparticles · micropipettes

[1] C. M. Sánchez-Sánchez, J. Rodríguez-López, A. J. Bard, *Anal. Chem.* **2008**, *80*, 3254–3260.
[2] a) M. Choi, L. A. Baker, *Anal. Chem.* **2018**, *90*, 11797–11801; b) C. Zhu, L. Zhou, M. Choi, L. A. Baker, *ChemElectroChem* **2018**, *5*, 2986–2990.
[3] a) M. Choi, N. P. Siepser, S. Jeong, Y. Wang, G. Jagdale, X. Ye, L. A. Baker, Probing Single-Particle Electrocatalytic Activity at Facet-Controlled Gold Nanocrystals *Nano Lett.* **2020**, accepted; b) N. Ebejer, M. Schnippering, A. W. Colburn, M. A. Edwards, P. R. Unwin, *Anal. Chem.* **2010**, *82*, 9141–9145.
[4] J. V. Macpherson, P. R. Unwin, *Anal. Chem.* **2000**, *72*, 276–285.
[5] C. Kranz, *Analyst* **2014**, *139*, 336–352.
[6] C. L. Bentley, M. Kang, P. R. Unwin, *Current Opinion in Electrochemistry* **2017**, *6*, 23–30.
[7] I. M. Ornelas, P. R. Unwin, C. L. Bentley, *Anal. Chem.* **2019**, Preprint.
[8] a) S. E. F. Kleijn, S. C. S. Lai, T. S. Miller, A. I. Yanson, M. T. M. Koper, P. R. Unwin, *J. Am. Chem. Soc.* **2012**, *134*, 18558–18561; b) J. Ustarroz, I. M. Ornelas, G. Zhang, D. Perry, M. Kang, C. L. Bentley, M. Walker, P. R. Unwin, *ACS Catal.* **2018**, *8*, 6775–6790; c) Y.-R. Kim, S. C. S. Lai, K.

McKelvey, G. Zhang, D. Perry, T. S. Miller, P. R. Unwin, *J. Phys. Chem. C* **2015**, *119*, 17389–17397.
[9] H. Böhni, T. Suter, A. Schreyer, *Electrochim. Acta* **1995**, *40*, 1361–1368.
[10] A. W. Hassel, M. M. Lohrengel, *Electrochim. Acta* **1997**, *42*, 3327–3333.
[11] a) T. Suter, H. Böhni, *Electrochim. Acta* **1998**, *43*, 2843–2849; b) L. Eng, E. Wirth, T. Suter, H. Böhni, *Electrochim. Acta* **1998**, *43*, 3029–3033; c) F. Assi, H. Böhni, *Wear* **1999**, *233–235*, 505–514.
[12] C. G. Williams, M. A. Edwards, A. L. Colley, J. V. Macpherson, P. R. Unwin, *Anal. Chem.* **2009**, *81*, 2486–2495.
[13] a) M. Dayeh, M. Ghavidel, J. Mauzeroll, S. Schougaard, *ChemElectroChem* **2018**, *6*; b) M. E. Snowden, M. Dayeh, N. A. Payne, S. Gervais, J. Mauzeroll, S. B. Schougaard, *J. Power Sources* **2016**, *325*, 682–689.
[14] D. Battistel, G. Pecchielan, S. Daniele, *ChemElectroChem* **2014**, *1*, 140–146.
[15] a) B. D. B. Aaronson, J. Garoz-Ruiz, J. C. Byers, A. Colina, P. R. Unwin, *Langmuir* **2015**, *31*, 12814–12822; b) S. Morsali, S. Daryadel, Z. Zhou, A. Behroozfar, D. Qian, M. Minary-Jolandan, *J. Appl. Phys.* **2017**, *121*, 024903; c) T. M. Day, P. R. Unwin, J. V. Macpherson, *Nano Lett.* **2007**, *7*, 51–57.
[16] J. A. Haber, Y. Cai, S. Jung, C. Xiang, S. Mitrovic, J. Jin, A. T. Bell, J. M. Gregoire, *Energy Environ. Sci.* **2014**, *7*, 682–688.
[17] a) J. W. Hill, C. M. Hill, *Nano Lett.* **2019**, *19*, 5710–5716; b) Y. Takahashi, A. Kumatani, H. Munakata, H. Inomata, K. Ito, K. Ino, H. Shiku, P. R. Unwin, Y. E. Korchev, K. Kanamura, T. Matsue, *Nat. Commun.* **2014**, *5*, 5450; c) H. Inomata, Y. Takahashi, D. Takamatsu, A. Kumatani, H. Ida, H. Shiku, T. Matsue, *Chem. Commun.* **2019**, *55*, 545–548; d) Y. Wang, E. Gordon, H. Ren, *J. Phys. Chem. Lett.* **2019**, *10*, 3887–3892; e) T. Tarnev, H. B. Aiyappa, A. Botz, T. Erichsen, A. Ernst, C. Andronescu, W. Schuhmann, *Angew. Chem. Int. Ed.* **2019**, *58*, 14265–14269; f) R. G. Mariano, K. McKelvey, H. S. White, M. W. Kanan, *Science* **2017**, *358*, 1187.
[18] a) S. Ranganathan, R. McCreery, S. M. Majji, M. Madou, *J. Electrochem. Soc.* **2000**, *147*, 277–282; b) R. L. McCreery, *Chem. Rev.* **2008**, *108*, 2646–2687; c) R. J. Bowling, R. T. Packard, R. L. McCreery, *J. Am. Chem. Soc.* **1989**, *111*, 1217–1223; d) K. C. Morton, H. Tokuhisa, L. A. Baker, *ACS Appl. Mater. Interfaces* **2013**, *5*, 10673–10681; e) K. C. Morton, C. A. Morris, M. A. Derylo, R. Thakar, L. A. Baker, *Anal. Chem.* **2011**, *83*, 5447–5452.
[19] P. Takmakov, M. K. Zachek, R. B. Keithley, P. L. Walsh, C. Donley, G. S. McCarty, R. M. Wightman, *Anal. Chem.* **2010**, *82*, 2020–2028.
[20] A. J. Gross, A. J. Downard, *Anal. Chem.* **2011**, *83*, 2397–2402.
[21] a) G. Sreenivas, S. S. Ang, I. Fritsch, W. D. Brown, G. A. Gerhardt, D. J. Woodward, *Anal. Chem.* **1996**, *68*, 1858–1864; b) H. X. He, Q. G. Li, Z. Y. Zhou, H. Zhang, S. F. Y. Li, Z. F. Liu, *Langmuir* **2000**, *16*, 9683–9686; c) D. Li, C. Batchelor-McAuley, L. Chen, R. G. Compton, *ACS Sens.* **2019**, *4*, 2250–2266.
[22] a) J. Heinze, *Angew. Chem. Int. Ed.* **1993**, *32*, 1268–1288; *Angew. Chem.* **1993**, *105*, 1327–1349; b) B. Ghane-Motlagh, M. Sawan, *2013 2nd International Conference on Advances in Biomedical Engineering*, **2013**, pp. 38–41; c) A. J. Bard, J. A. Crayston, G. P. Kittlesen, T. Varco Shea, M. S. Wrighton, *Anal. Chem.* **1986**, *58*, 2321–2331; d) D. Lowinsohn, H. E. M. Peres, L. Kosminsky, T. R. L. C. Paixão, T. L. Ferreira, F. J. Ramirez-Fernandez, M. Bertotti, *Sens. Actuators B* **2006**, *113*, 80–87; e) P. N. Bartlett, S. L. Taylor, *J. Electroanal. Chem.* **1998**, *453*, 49–60.
[23] a) C. G. Zoski, N. Simjee, O. Guenat, M. Koudelka-Hep, *Anal. Chem.* **2004**, *76*, 62–72; b) Z. Lin, Y. Takahashi, Y. Kitagawa, T. Umemura, H. Shiku, T. Matsue, *Anal. Chem.* **2008**, *80*, 6830–6833.
[24] J. Guo, E. Lindner, *Anal. Chem.* **2009**, *81*, 130–138.
[25] S. C. S. Lai, A. N. Patel, K. McKelvey, P. R. Unwin, *Angew. Chem. Int. Ed.* **2012**, *51*, 5405–5408; *Angew. Chem.* **2012**, *124*, 5501–5504.
[26] D. Martín-Yerga, A. Costa-García, P. R. Unwin, *ACS Sens.* **2019**, *4*, 2173–2180.
[27] a) D. Momotenko, J. C. Byers, K. McKelvey, M. Kang, P. R. Unwin, *ACS Nano* **2015**, *9*, 8942–8952; b) L. C. Yule, V. Shkirskiy, J. Aarons, G. West, C. L. Bentley, B. A. Shollock, P. R. Unwin, *J. Phys. Chem. C* **2019**, *123*, 24146–24155.
[28] D. Britz, J. Strutwolf, *Electrochim. Acta* **2006**, *52*, 33–41.
[29] a) A. M. Bond, D. Luscombe, K. B. Oldham, C. G. Zoski, *J. Electroanal. Chem. Interfacial Electrochem.* **1988**, *249*, 1–14; b) C. Amatore, A. I. Oleinick, I. Svir, *J. Electroanal. Chem.* **2006**, *597*, 69–76.
[30] A. J. Bard, L. R. Faulkner, *Electrochemical Methods*, John Wiley, New York, **2001**.
[31] J. Xiao, S. Liu, N. Tian, Z.-Y. Zhou, H.-X. Liu, B.-B. Xu, S.-G. Sun, *J. Am. Chem. Soc.* **2013**, *135*, 18754–18757.
[32] K. Huang, J. Clausmeyer, L. Luo, K. Jarvis, R. M. Crooks, *Faraday Discuss.* **2018**, *210*, 267–280.
[33] a) F. J. Vidal-Iglesias, R. M. Arán-Ais, J. Solla-Gullón, E. Herrero, J. M. Feliu, *ACS Catal.* **2012**, *2*, 901–910; b) B. D. B. Aaronson, S. C. S. Lai, P. R. Unwin, *Langmuir* **2014**, *30*, 1915–1919.
[34] S. Trasatti, O. A. Petrii, *J. Electroanal. Chem.* **1992**, *327*, 353–376.
[35] N. Tian, Z.-Y. Zhou, S.-G. Sun, Y. Ding, Z. L. Wang, *Science* **2007**, *316*, 732.
[36] Z.-Y. Zhou, N. Tian, Z.-Z. Huang, D.-J. Chen, S.-G. Sun, *Faraday Discuss.* **2009**, *140*, 81–92.

Manuscript received: November 25, 2019
Revised manuscript received: December 19, 2019
Accepted manuscript online: January 9, 2020